

Genetic Interactions between Doublecortin and Doublecortin-like Kinase in Neuronal Migration and Axon Outgrowth

Thomas A.S. Deuel,^{1,3} Judy S. Liu,^{1,3}
Joseph C. Corbo,^{1,4} Seung-Yun Yoo,¹
Lucy B. Rorke-Adams,² and Christopher A. Walsh^{1,*}

¹Howard Hughes Medical Institute
Beth Israel Deaconess Medical Center
Division of Genetics
Children's Hospital and
Department of Neurology and Program in Neuroscience
Harvard Medical School
Boston, Massachusetts 02115

²Department of Pathology
The Children's Hospital of Philadelphia
34th Street and Civic Center Boulevard
Philadelphia, Pennsylvania 19104

Summary

Although mutations in the human doublecortin gene (*DCX*) cause profound defects in cortical neuronal migration, a genetic deletion of *Dcx* in mice produces a milder defect. A second locus, doublecortin-like kinase (*Dclk*), encodes a protein with similar “doublecortin domains” and microtubule stabilization properties that may compensate for *Dcx*. Here, we generate a mouse with a *Dclk* mutation that causes no obvious migrational abnormalities but show that mice mutant for both *Dcx* and *Dclk* demonstrate perinatal lethality, disorganized neocortical layering, and profound hippocampal cytoarchitectural disorganization. Surprisingly, *Dcx*^{-y};*Dclk*^{-/-} mutants have widespread axonal defects, affecting the corpus callosum, anterior commissure, subcortical fiber tracts, and internal capsule. *Dcx*/*Dclk*-deficient dissociated neurons show abnormal axon outgrowth and dendritic structure, with defects in axonal transport of synaptic vesicle proteins. *Dcx* and *Dclk* may directly or indirectly regulate microtubule-based vesicle transport, a process critical to both neuronal migration and axon outgrowth.

Introduction

The doublecortin gene (*DCX*), which encodes a microtubule-associated protein, is essential for normal human brain development because mutations in *DCX* cause X-linked lissencephaly (XLIS) (des Portes et al., 1998; Gleeson et al., 1998). XLIS males have severe mental retardation, seizures, and a shortened lifespan. Affected individuals lack doublecortin function and have lissencephaly in which the cortical surfaces are abnormally smooth and the cortex itself is abnormally thick with a paucity of white matter (Berg et al., 1998; Dobyns et al., 1996). Though females heterozygous for *DCX* have

milder clinical features than affected males, most still suffer from mental retardation and seizures. Affected females have “double cortex” syndrome with a relatively normal cerebral cortex and a second layer of gray matter within the subcortical white matter called a subcortical band heterotopia. Thus, *DCX* is strongly implicated in having a critical role in the migration of cerebral cortical neurons.

The *DCX* gene encodes a microtubule associated protein (MAP) that is expressed primarily in post mitotic neurons during cortical development, both during periods of neuronal migration as well as during neurite formation (Francis et al., 1999; Gleeson et al., 1999). The *DCX* protein binds to microtubules and stimulates polymerization (Francis et al., 1999; Gleeson et al., 1999). Disease-causing missense mutations in the *DCX* gene affect amino acids that cluster within two domains required for *Dcx* binding to tubulin (Taylor et al., 2000), now recognized as “doublecortin domains,” representing the microtubule binding domains (Kim et al., 2003).

Surprisingly, the *Dcx* mouse mutant (Corbo et al., 2002) has normal appearing neocortical lamination, though there is disrupted layering in the hippocampus, and the males usually die postnatally. In contrast, acute “knockdown” of *Dcx* mRNA with RNAi constructs can cause a migrational arrest of cortical neurons beneath the cortical plate in rats (Bai et al., 2003). Although there are many possibilities for these conflicting results (e.g., species differences and technical differences) we have focused on the possibility that loss of *Dcx* may be functionally compensated for by other genes in the mouse.

Doublecortin-like kinase (*Dclk*) is the gene most similar to *Dcx*, with 78% amino acid identity between the N-terminal ends containing the doublecortin domains. However, unlike *Dcx*, *Dclk* also encodes a kinase domain in the C terminus of the protein (Burgess et al., 1999). *Dclk* also functions as a MAP. The N-terminal doublecortin domain of *Dclk* binds to microtubules and stimulates microtubule polymerization (Lin et al., 2000; Silverman et al., 1999). The C-terminal kinase domain phosphorylates myelin basic protein and itself in vitro, though in vivo substrates of *Dclk* are unknown (Lin et al., 2000; Silverman et al., 1999). Like *Dcx*, *Dclk* is expressed in the mouse embryo starting at embryonic day 11 (E11) in the brain (Burgess and Reiner, 2000; Sossey-Alaoui and Srivastava, 1999), but unlike *Dcx*, the *Dclk* locus encodes multiple, different transcripts, some of which are expressed in the adult or in response to neural activity suggesting *Dclk* may have additional functions beyond neural development (Burgess et al., 1999; Burgess and Reiner, 2002; Hevroni et al., 1998; Silverman et al., 1999; Vreugdenhil et al., 1999).

Here, we used homologous recombination in ES cells to create a targeted mutation in *Dclk*. *Dclk* single mutants are viable with grossly normal brain architecture. *Dcx*^{-y};*Dclk*^{-/-} double mutants suffer severe perinatal lethality and show severe defects in major axonal tracts as well as disruption of hippocampal laminar structure that is more severe than that seen in the *Dcx*

*Correspondence: cwals@bidmc.harvard.edu

³These authors contributed equally to this work.

⁴Present address: Department of Pathology and Immunology, Washington University School of Medicine, Campus Box 8118, 660 South Euclid Avenue, St. Louis, Missouri 63110.

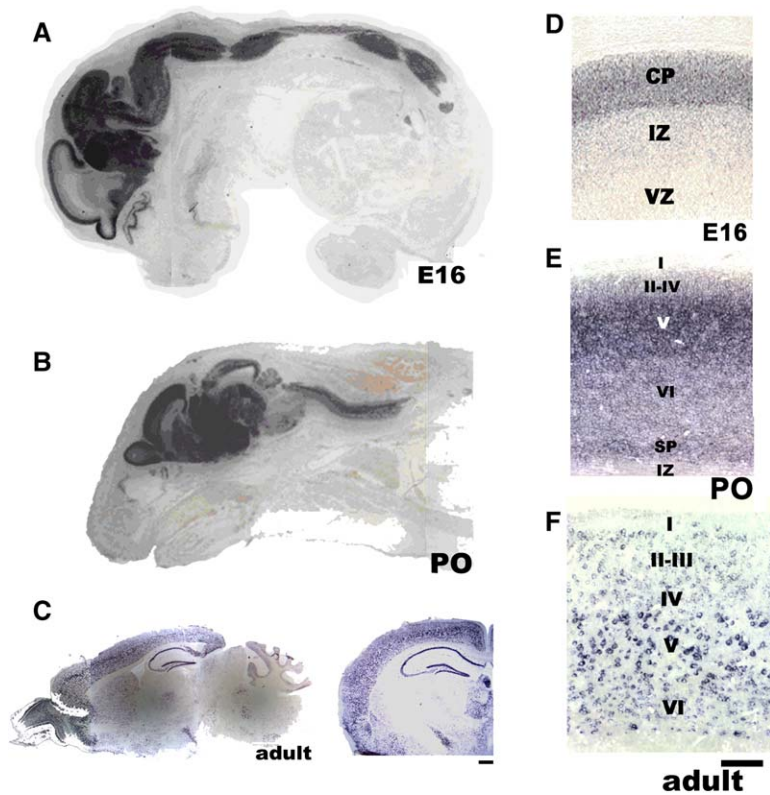


Figure 1. *Dclk* Expression

(A) A parasagittal section of an E16 embryo shows widespread expression of *Dclk* in the CNS.

(B) A parasagittal section of a P0 embryo shows expression of *Dclk* in the brain and spinal cord persisting at high levels.

(C) Adult whole brain sagittal (left) and coronal (right) sections show persistent cortical, hippocampal, and cerebellar expression, lower expression in the basal ganglia, and very little *Dclk* expression in the thalamus.

(D–F) High power views of the cortex at E16, P0, and adult stages demonstrate expression of *Dclk* in the dense cortical plate (CP) at E16 and predominantly in layer V at P0 and adult stages. (Scale bars are 4 mm in [A], [B], and [C] and 100 μ m in [D], [E], and [F]).

knockout alone. Moreover, the cerebral neocortex of these animals shows abnormal neuronal lamination. These data show that *Dcx* and *Dclk* have genetically compensatory roles in neuronal migration but also uncover roles for both of these proteins in axon outgrowth as well.

Results

Expression of *Dclk* mRNA during Development

Using in situ hybridization with a probe for the 3'UTR of *Dclk* designed to recognize most *Dclk* transcripts (see [Experimental Procedures](#)), we confirmed the widespread expression of *Dclk* throughout the developing and adult CNS. Hybridization was seen in tissues throughout the CNS ([Figures 1A–1C](#)), including developing cerebral cortex, olfactory bulbs, and olfactory epithelium, as well as midbrain, pons, cerebellum, medulla, and spinal cord beginning on E12. In the developing cerebral cortex, expression was seen mainly in the cortical plate that contains postmitotic, postmigratory neurons. However, there were lower levels of expression in the intermediate zone—confirmed by immunohistochemistry to the protein ([Lin et al., 2000](#))—whereas little to no expression was seen in the ventricular zone ([Figure 1D](#)). In the postnatal day zero (P0) and adult brain ([Figures 1E and 1F](#)), expression persisted in cortical layers II–VI, with highest expression in layer V neurons whose axons make up the efferent long tracts. Expression also persisted in the olfactory bulb, hippocampus, striatum, and cerebellum ([Figure 1C](#)), but relatively little expression was seen in the rest of the CNS including the thalamus.

Targeted Mutagenesis of the Mouse *Dclk* Locus

To simultaneously target the multiple *Dclk* transcripts, we designed a targeting construct to delete exons 9–11 because these encode the core of the kinase domain and are also contained in virtually all known *Dclk* transcripts ([Figures 2A and 2B](#)). This construct introduced a frame shift that generated multiple stop codons downstream of exon 9 ([Figure 2A](#)). The *Dclk* gene produces: (1) *Dclk* β and *Dclk* α full-length transcripts, coding for proteins including the doublecortin and the kinase domain; (2) a doublecortin domain transcript (*Dcl*) that does not encode most of the kinase domain; (3) a kinase-domain only transcript (*cpk16*); and (4) CARP, which encodes neither the doublecortin nor the kinase domain ([Burgess and Reiner, 2002](#); [Silverman et al., 1999](#); [Vreugdenhil et al., 1999](#)). The targeting construct should disrupt all transcripts except for Ca^{2+} /calmodulin-dependent protein kinase (CaMK)-related peptide (CARP).

200 targeted ES cell colonies were screened by Southern blot (see [Experimental Procedures](#)) for homologous recombination. Four positive ES cell clones were identified, and two were independently injected into blastocysts, which were then implanted to produce agouti chimeric males. Chimeras were crossed to wild-type animals to generate *Dclk*^{+/-} mice. Interbreeding of heterozygous animals produced *Dclk*^{-/-} mutants.

We examined *Dclk* protein by performing Western blot analysis on brain protein with two antisera raised against the N terminus ([Lin et al., 2000](#); [Mizuguchi et al., 1999](#)) and one against the C terminus ([Burgess et al., 1999](#)). In the wild-type (wt) mouse both the N-terminal and C-terminal antisera detected an 85 kDa doublet, likely representing either two phosphorylated isoforms of

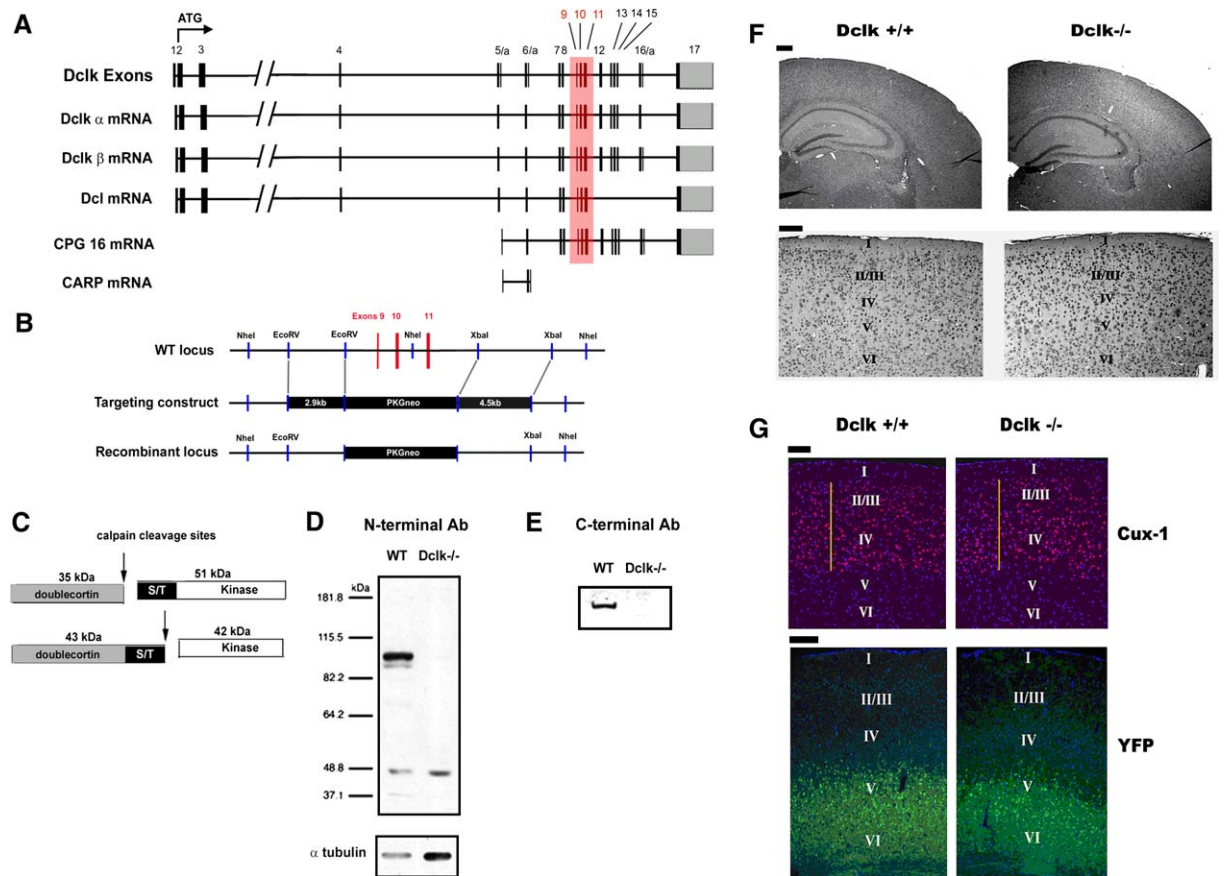


Figure 2. *Dclx*-Targeting Construct and Histology of *Dclx*^{-/-} Mouse

(A) Intron/exon structure of *Dclx* (modified from Burgess and Reiner [2002]) and consequences of elimination of exons 9–11 (note that exon numbering system is based on the UCSC Genome database, which is different than that of Burgess and Reiner [2002]). The targeting construct replaces exons 9–11 with a PKG neo cassette, which introduces a translational frame shift, resulting in multiple stop codons 3' of exons 9–11. All transcripts except CARP should thus be targeted.

(B) The PGK-neo cassette replaces exons 9–11 of *Dclx* genomic DNA and *NheI/EcoRV* fragment was used to screen *NheI* digested DNA from ES cell colonies for an 11.7 kb mutant band in addition to the 5.7 kb wt fragment by Southern blot analysis.

(C) *Dclx* is cleaved by calpain at two different sites, resulting in two different N-terminal fragments of 35 kDa and 43 kDa (adapted from Burgess and Reiner [2002]).

(D) Western analysis of *Dclx*^{-/-} mutants shows the full-length 85 kDa *Dclx* protein is present only in wild-type, but calpain cleaved proteolytic products (43 kDa and 35 kDa) are seen in *Dclx*^{-/-} as well as wt. α -tubulin antibody was used as a loading control. Note that the *Dclx*^{-/-} lane is heavily overloaded in order to detect the residual smaller fragments.

(E) Full-length *Dclx* protein is undetectable in *Dclx*^{-/-} brain by C-terminal antibody.

(F) Normal gross brain architecture and lamination in *Dclx*^{-/-} mice. Hematoxylin and eosin (H&E) histology of coronal sections from adult wild-type and *Dclx*^{-/-} mice show normal overall brain histology.

(G) Adult wt and *Dclx*^{-/-} mice demonstrate normal lamination with layer-specific markers. Cux-1 immunohistochemistry of coronal sections from adult wild-type and *Dclx*^{-/-} mice show indistinguishable distribution of Cux-1 positive neurons in layers II–IV. *thy1*-YFP labeling of layer V pyramidal neurons shows normal distribution of neurons in layer V in *Dclx*^{-/-} and control cortex. (Scale bars are 400 μ m in [F] and 100 μ m in other panels.)

Dclx or the *Dclx* α and β splice variants. The full-length protein, which made up 83% of all isoforms encoding doublecortin domains in wt animals, was not detected in *Dclx*^{-/-} mice (Figures 2D and 2E). Calpain cleavage of the full-length protein produced N-terminal products 43 and 35 kDa in size (Burgess and Reiner, 2001), which made up 15.3% and 1.6%, respectively, of the doublecortin domain encoding isoforms in normal mice. Although the major 85 kDa isoform of *Dclx* was not seen in homozygous mutants, faint bands representing the N-terminal calpain cleavage products could be seen. Although these products may be functional, they were much less abundant than full-length *Dclx* protein in the wt mouse. In total, in the *Dclx* homozygous mutant

mouse, less than 10% (8.7%) of products detected by the N-terminal antibody remained. Moreover, the absence of detectable protein with the C-terminal antibody in the mutant (Figure 2E) confirms elimination of all kinase domain isoforms.

Preserved Neocortical Architecture and Viability in *Dclx* Mutant Mice

Dclx mutant animals were born in approximately Mendelian ratios with normal survival and fertility. Mutants were indistinguishable in appearance and behavior from wild-type littermates. No spontaneous seizures were observed in the mutant animals. Histological analysis (Figure 2F) revealed normal gross brain architecture.

The striatum, thalamus, hippocampus, and cerebellum also appeared normal. *Dclk*^{-/-} mice had a normally laminated cerebral cortex. Overall cortical thickness was indistinguishable between mutants and wild-type mice, as was the thickness of the individual layers. There was no evidence of periventricular or white matter neuronal heterotopia in the mutant mice by routine histology.

Neocortical layer-specific markers also confirmed that cortical layering was preserved in *Dclk*^{-/-} mice. *Cux-1* immunoreactivity, which localizes to layers II–IV of the neocortex (Nieto et al., 2004) (Figure 2G); *Foxp1* immunoreactivity, which identifies layers III–V; and *Foxp2* immunoreactivity, which identifies neurons in layer VI (Ferland et al., 2003) (data not shown), were indistinguishable from wt. Lamination was further examined by using a transgenic mouse that expresses yellow fluorescent protein (YFP) under the control of a *thy1* enhancer and in which YFP is expressed predominantly in a subset of layer V neurons (Feng et al., 2000a). In homozygous mutants, labeled pyramidal neurons in layer V neurons showed a sharp laminar organization that was indistinguishable from wild-type (Figure 2G). These studies suggest that the overall structure of the neocortex of *Dclk* mutant mice is normal and that the mutant mice have no obvious defects in neuronal migration, although more subtle defects in axon targeting, axon growth, or plasticity related phenotypes have not been ruled out by this analysis.

Perinatal Lethality and Abnormal Brain Architecture in *Dcx*^{-/-};*Dclk*^{-/-} Mice

Because humans with *DCX* mutations show such striking cortical development abnormalities and neither the *Dcx* nor *Dclk* mutant mice alone show neocortical lamination defects, we generated double mutant (*Dcx*^{+/-};*Dclk*^{-/-}) mice to test whether the two genes might compensate for each other in cerebral cortex layer formation. We bred *Dcx*^{+/-};*Dclk*^{+/-} females with *Dclk*^{-/-} males to generate *Dcx*^{+/-};*Dclk*^{-/-} mice. These crosses would be expected to produce offspring in a ratio of 2:2:1:1:1:1 (Table 1). Although the offspring were born in approximately the expected Mendelian ratios, more than 3/4 of the (*Dcx*^{-/-};*Dclk*^{-/-}) die postnatally, usually within 2 days of birth (Table 1). A slightly smaller proportion of the *Dcx*^{-/-};*Dclk*^{+/-} mice die postnatally as well. *Dcx*^{+/-};*Dclk*^{+/-} and *Dcx*^{+/-};*Dclk*^{-/-} females appear to survive relatively normally, however, they have reduced fertility as adults.

Dcx/Dclk double mutant animals (*Dcx*^{-/-};*Dclk*^{-/-}) showed severely abnormal brain architecture (Figures

3, 4A, and 5). Histological analysis of the brain at P0 demonstrated a brain with a thin cerebral cortex (Figures 3A, 4A, and 5B), disruption of lamination in the cingulate gyrus, and markedly abnormal cell layering in the hippocampus (Figures 3A, 4A, and 5E). The *Dcx*^{-/-};*Dclk*^{-/-} mutant also had severely disorganized white-matter tracts (Figures 3A and 5) with disruption of many thalamic and brainstem nuclei (Figure 3A), as well as a small cerebellum with defective foliation (Figure 3B), despite a relatively normal appearing external granule layer and Purkinje cell layer at higher power (not shown). Coronal sections of the double mutant (*Dcx*^{-/-};*Dclk*^{-/-}) as well as *Dcx*^{-/-};*Dclk*^{+/-} mice showed enlargement of the lateral ventricles (Figures 5A and 5B).

Defective Neuronal Migration in *Dcx*^{-/-};*Dclk*^{-/-} Double Mutant Mice

The hippocampus of the double mutant (*Dcx*^{-/-};*Dclk*^{-/-}) mouse at P0 was cytoarchitecturally disrupted (Figure 4A). The lamination defects of the hippocampus were much more severe than those previously seen in the *Dcx* single knockout animal (Corbo et al., 2002) and appeared similar to hippocampal defects seen in *Cdk5*^{-/-} animals (Ohshima et al., 1996). Like the *Cdk5* mutant, cells appeared less tightly packed in the dentate gyrus, with little or no layering of cells in a granule cell layer per se but instead dispersion of neuronal cell bodies throughout the dentate gyrus. The stratum pyramidale (SP) layer in pyramidal cell fields, CA3, CA2, and CA1 was disorganized with multiple layers separated by irregular streams of white matter in no consistent pattern. The cingulate cortex in some areas appeared to be split, with two or three irregular layers of cells separated by irregular cell-free zones (Figure 4A), in contrast to *Dcx* and *Dclk* single knockout animals, which had no apparent neocortical defects.

Although the lateral parts of the *Dcx*^{-/-};*Dclk*^{-/-} double mutant neocortex (Figure 4A) were more mildly disrupted compared to *Dclk*^{-/-} or wild-type brains (not shown) by H&E staining or cresyl violet staining, closer examination of lateral neocortex with layer-specific markers at age P0 revealed laminar disorganization (Figure 4B and Figure S1B). In contrast to the *Dclk*^{-/-} and *Dcx*^{-/-};*Dclk*^{+/-} mutants, *Cux-1* immunoreactivity, showed some dispersion of labeled layer II–IV neurons (Nieto et al., 2004) into deeper neocortical layers in the *Dcx*^{-/-};*Dclk*^{-/-} double mutant. Layer III–V neurons labeled with *Foxp1* (Ferland et al., 2003) were also more loosely packed than controls, indicating defects in migration of neurons that form these cortical layers. Limited BrdU analysis at P0, after injection at E12 (data not shown) and E16 (Figure S1A) also showed mild dispersion of upper layer neurons into deeper neocortical layers and intermediate zone.

Although layer-specific markers revealed laminar disorganization, analysis of the marginal zone and subplate did not show a defect in preplate splitting—a process that is disrupted in some migration disorders (Caviness, 1982). G10 immunoreactivity (Reelin, layer I) (Figure 4C) demonstrates Reelin-positive cells in the marginal zone (MZ) (de Bergeyck et al., 1998), although in 2/5 animals examined, the MZ appeared thinner in the *Dcx*^{-/-};*Dclk*^{-/-} mouse and cells appeared smaller than the littermate control (*Dclk*^{+/-}). However, in other *Dcx*^{-/-};*Dclk*^{-/-} double mutants with abnormal migration, the MZ

Table 1. Offspring of *Dcx*^{+/-};*Dclk*^{+/-} × *Dclk*^{-/-}

	<i>Dcx</i> wt <i>Dclk</i> ^{+/-}	<i>Dcx</i> wt <i>Dclk</i> ^{-/-}	<i>Dcx</i> ^{+/-} <i>Dclk</i> ^{+/-}	<i>Dcx</i> ^{+/-} <i>Dclk</i> ^{-/-}	<i>Dcx</i> ^{-/-} <i>Dclk</i> ^{+/-}	<i>Dcx</i> ^{-/-} <i>Dclk</i> ^{-/-}
P0	17	13	4	8	7	10
18 days	13	19	7	9	4	2
Expected ratio	2	2	1	1	1	1

Pre- and postnatal lethality of *Dcx*^{-/-};*Dclk*^{-/-} double knockout mice. Total number of mice from *Dcx*^{+/-};*Dclk*^{+/-} × *Dclk*^{-/-} matings of each genotype at ages P0 and P18 are shown. Expected ratios are 2:2:1:1:1:1. *Dcx* wt represents both *Dcx*^{+/-} males and *Dcx*^{+/-} females.

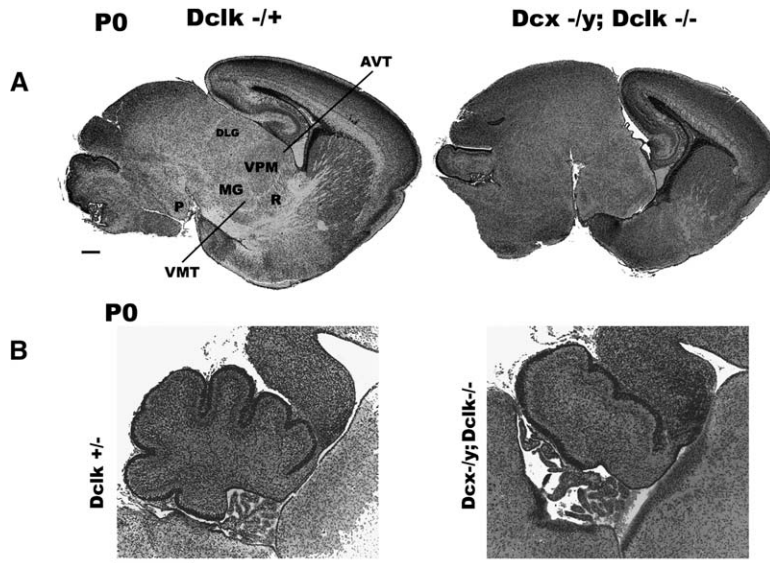


Figure 3. Neocortical, Hippocampal, Cerebellar, and Axonal Defects in *Dcx*^{-ly};*Dclk*^{-ly-ly} Mice at P0

(A) A sagittal section of the *Dcx*^{-ly};*Dclk*^{-ly-ly} mutant mouse shows abnormalities in the neocortex, hippocampus, white-matter tracts, and cerebellum as compared to *Dclk*^{-ly} control. Nuclei of the thalamus and brainstem are clearly seen in the control but not in the *Dcx*^{-ly};*Dclk*^{-ly-ly} mutant mouse, including the anterior ventral thalamic nucleus (AV), dorsal lateral geniculate body (DLG), medial geniculate body (MG), reticular thalamic nucleus (R), pontine nuclei (P), ventral posterior nucleus of the thalamus, medial part (VPM), and ventromedial thalamic nucleus (VM).

(B) The *Dcx*^{-ly};*Dclk*^{-ly-ly} mouse cerebellum is smaller than control and demonstrate defective folia. Although the folia are mainly present in the *Dcx*^{-ly};*Dclk*^{-ly-ly} mutant, they are severely hypoplastic, especially on the ventral surface of the cerebellum. (Scale bars are 400 μm.)

appeared normal, so that the significance of this is unclear. Chondroitin sulfate immunoreactivity demonstrated normal preplate splitting with intense immunoreactivity in the marginal zone and subplate of the *Dcx*^{-ly};*Dclk*^{-ly-ly} double mutant that was indistinguishable from the control (Figure 4C).

Defective White-Matter Tracts in *Dcx*^{-ly};*Dclk*^{-ly-ly} Double Mutant Mice

Unlike either the *Dcx* or *Dclk* single mutant animals, *Dcx*^{-ly};*Dclk*^{-ly-ly} mice were notable for disruption of most or all major axon tracts in the brain including the corpus callosum, hippocampal commissures, anterior commissure, and internal capsule (Figures 3 and 5). In the sagittal sections shown (Figure 3A), there was a striking absence of an internal capsule and pencil fibers in the striatum, as well as a global disorganization of the nuclear structure of the thalamus and brainstem because of the paucity of white-matter tracts in the double mutant as compared to the control. In the same sagittal sections, the individual thalamic nuclei that are clearly discernable in control sections—including the anterior ventral thalamic nucleus (AV), dorsal lateral geniculate body (DLG), medial geniculate body (MG), reticular thalamic nucleus (R), ventral posterior nucleus of the thalamus, medial part (VPM), and ventromedial thalamic nucleus (VM)—are not demarcated in the double mutant. In the brainstem, the pontine nuclei (P) are seen in control sections but not clearly defined in the *Dcx*^{-ly};*Dclk*^{-ly-ly} mouse. Four out of six mice examined showed the global disruption of white-matter tracts seen in Figure 3A, and two of the six *Dcx*^{-ly};*Dclk*^{-ly-ly} mutants examined were more mildly affected. The horizontal section from a more mildly affected *Dcx*^{-ly};*Dclk*^{-ly-ly} animal in Figure 5H shows diffuse fibers of the anterior commissure that do not cross the midline; in contrast the internal capsule in this same animal is less severely defective than that illustrated in Figure 5E.

The corpus callosum of *Dcx*^{-ly};*Dclk*^{-ly-ly} mutants was present at rostral levels but did not extend as far caudally as in wt mice. In a coronal section taken at the level of the crossing of the anterior commissure, the *Dcx*^{-ly};*Dclk*^{-ly-ly}

mice showed no fibers crossing the midline in the corpus callosum (Figure 5B), whereas the comparable *Dclk*^{-ly-ly} brain (Figure 5A) shows the normal corpus callosum present at a comparable plane of section. Although the anterior portion of the corpus callosum was present in the *Dcx*^{-ly};*Dclk*^{-ly-ly} mutant, it was greatly reduced in thickness (not shown). In these double mutant mice, white-matter tracts just lateral to the corpus callosum showed disorganized swirls (Figure 5I), similar to Probst bundles. The hippocampal commissures and subcortical white matter appeared lumpy and disorganized (Figures 5B and 5I). Moreover, the striatum in *Dcx*^{-ly};*Dclk*^{-ly-ly} double mutant animals was devoid of normal pencil fibers (Figures 5A and 5B). Additionally, the anterior commissure failed to cross at the midline in the *Dcx*^{-ly};*Dclk*^{-ly-ly} double mutant brain (Figures 5A and 5B) and could not be seen at all at most levels where it normally is found. Instead, aberrant, diffuse axonal bundles that fail to follow their normal course were seen stemming from the areas normally giving rise to the anterior commissure (marked by an arrow in Figures 5B and 5H).

Mice with a *Dcx*^{-ly};*Dclk*^{+ly-ly} genotype also had white matter defects (Figures 5C and 5F), but these were generally less severe and less highly penetrant than in *Dcx*^{-ly};*Dclk*^{-ly-ly} mice. Of six *Dcx*^{-ly};*Dclk*^{+ly-ly} mice examined, three showed white-matter abnormalities beyond those expected based on the *Dcx* genotype alone (Corbo et al., 2002). Figure 5C shows absence of the corpus callosum, and the aberrant anterior commissure bundles and Figure 5F shows a markedly abnormal internal capsule on coronal section. In contrast to the *Dcx*^{-ly};*Dclk*^{-ly-ly} mutants, *Dcx*^{-ly};*Dclk*^{+ly-ly} mice have few or no defects in lamination (Figures 4A and 4B). The presence of axonal tract defects without observable migration problems in *Dcx*^{-ly};*Dclk*^{+ly-ly} mutants suggests that defects in axon tract formation and neuronal migration are partially separable phenotypes and that the migration phenotypes are not secondary to the axonal ones, or vice versa.

P0 brains received Dil injections in order to label axon bundles to characterize the white-matter tracts in the double mutants in more detail (Figure 6). In the *Dcx*^{-ly};*Dclk*^{-ly-ly} double mutant, the anterior commissure was

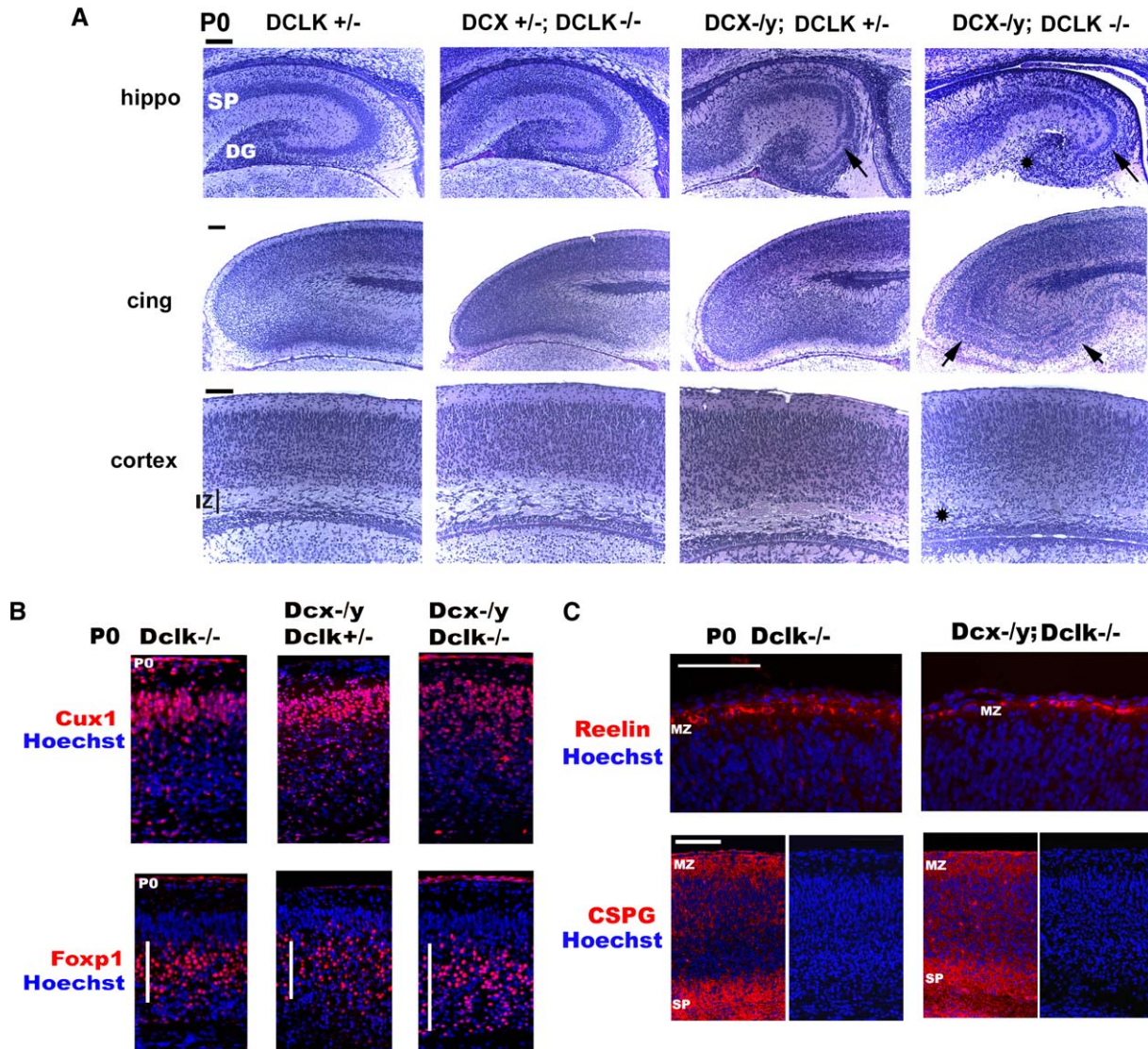


Figure 4. Lamination Defects in *Dcx^{-ly};Dclk^{-/-}* Mice

(A) H&E histology of coronal sections from P0 *Dclk^{-/-}* and *Dcx^{-ly};Dclk^{-/-}* mice. The hippocampus of the *Dcx^{-ly};Dclk^{+/-}* mouse and the double mutant *Dcx^{-ly};Dclk^{-/-}* shows disruption of lamination with more severe defects in the double mutant (hippo). The stratum pyramidale (SP) and the dentate gyrus (DG) appear normal in the *Dclk^{+/-}*, and *Dcx^{+/-};Dclk^{-/-}* mutants; however, in the *Dcx^{-ly};Dclk^{+/-}* and more severely in the *Dcx^{-ly};Dclk^{-/-}* mutant, the pyramidal cell layer is dispersed with neurons separated by cell-free zones (arrows). The dentate gyrus also appears much less organized and much less distinct in the *Dcx^{-ly};Dclk^{-/-}* mutant (star). The cingulate cortex shows gross disorganization and splitting in the *Dcx^{-ly};Dclk^{-/-}* double mutant but not in other genotype mice (cing). The lateral cerebral cortex looks relatively well preserved in the double mutant as compared to other littermate controls; however, the intermediate zone in the double mutant is less well defined and shows arrested cells (cortex). (Scale bars are all 100 μ m.)

(B) Lamination is abnormal in the *Dcx^{-ly};Dclk^{-/-}* mouse. Cux-1 (layers II–IV) immunoreactive cells are less tightly packed in the upper layers of the *Dcx^{-ly};Dclk^{-/-}* cortex at P0 as compared to *Dcx^{-ly};Dclk^{+/-}* and *Dclk^{-/-}* mice suggesting abnormal migration of upper cortical plate layers. Foxp1 (layers III–V) immunoreactivity of the *Dcx^{-ly};Dclk^{-/-}* mouse shows dispersed cellular layering as well compared to littermate controls. (C) *Dcx^{-ly};Dclk^{-/-}* mutant mice show no clear defects in preplate splitting. G10 (Reelin, layer I) staining is relatively normal in *Dcx^{-ly};Dclk^{-/-}* double mutants, though the marginal zone in some mice appears somewhat thinner than normal. Chondroitin sulfate proteoglycan staining is indistinguishable in the *Dcx^{-ly};Dclk^{-/-}* double mutant from the *Dclk^{-/-}* mouse. (Both scale bars in [C] represent a size of 100 μ m, and the scale bar on the lower panel applies to the panels in [B] as well).

absent with no axons leaving the area of the entorhinal cortex (Figure 6A). In the *Dcx^{-ly};Dclk^{-/-}* double mutant, most axons forming the caudal corpus callosum ended before reaching midline and did not cross to the other side, in contrast to the normally crossing fibers observed in the *Dclk* heterozygote littermate control (Figure 6B). Under high magnification (60 \times), the normal axons are arranged in discrete fascicles with a consis-

tent orientation. In contrast to the control littermate, the axons of the double knockout did not travel in bundles but instead appeared as multiple single axons with what appeared to be random orientation and without clear fasciculation (Figure 6C).

In order to confirm a role for human DCX in axon outgrowth and to compare the axons from human neurons without functional DCX to the mouse mutant, we studied

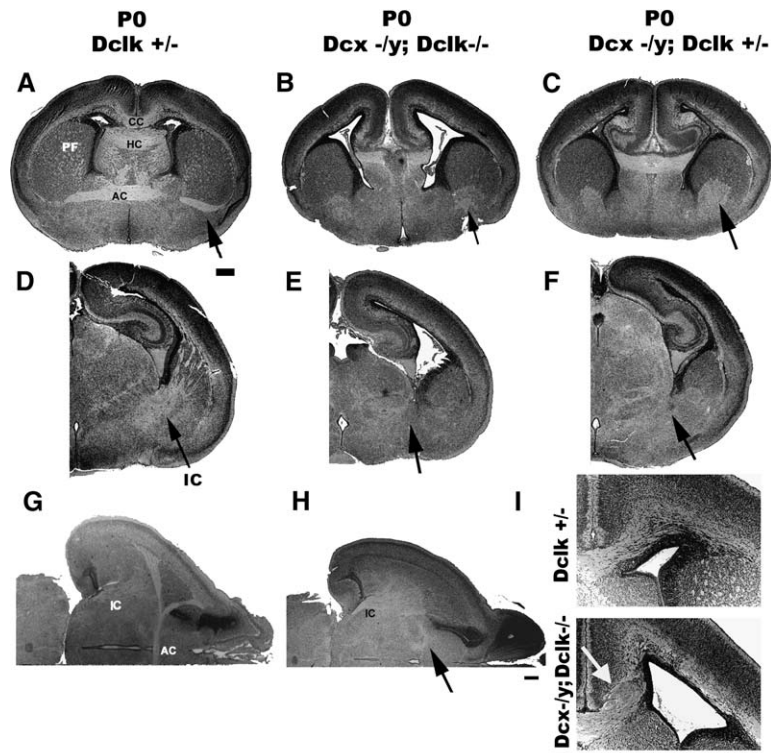


Figure 5. Axonal Defects in Both *Dcx*^{-/-}; *Dclk*^{-/-} and *Dcx*^{-/-}; *Dclk*^{+/-} Mutants at P0
(A) A coronal section of the *Dclk*^{+/-} mouse demonstrates the normal appearance of the corpus callosum (CC) and anterior commissure (AC), hippocampal commissures (HC), and pencil fibers in the striatum (PF). (B and C) In contrast, the corpus callosum is not present at the level represented in the control section in either the *Dcx*^{-/-}; *Dclk*^{-/-} (B) or the *Dcx*^{-/-}; *Dclk*^{+/-} (C) mutant. Furthermore, anterior commissure fibers fail to turn and cross the midline in these sections. Instead aberrant bundles are seen (arrows). The *Dcx*^{-/-}; *Dclk*^{-/-} striatum is almost devoid of pencil fibers, and the hippocampal commissure appears abnormal as well. (D) Caudal coronal sections of the *Dclk*^{+/-} mouse demonstrate a relatively intact internal capsule (IC). (E and F) However, the internal capsule (arrows) appears to be severely abnormal in the *Dcx*^{-/-}; *Dclk*^{-/-} (E) and the *Dcx*^{-/-}; *Dclk*^{+/-} (F) mutants. (G) A ventral horizontal section of the *Dclk*^{+/-} control demonstrates an intact internal capsule (IC), as well as normal anterior commissure fibers crossing the midline (AC). (H) In contrast, the *Dcx*^{-/-}; *Dclk*^{-/-} mutant shows anterior commissure fibers that fail to cross the midline normally (arrow), though in this double mutant the defect in internal capsule (IC) is extremely mild compared to that in the double mutant illustrated in (B). (I) Higher magnification shows abnormal subcortical white matter of the *Dcx*^{-/-}; *Dclk*^{-/-} double mutant in comparison to that of the control. The arrow indicates a Probst bundle. (Scale bars are all 400 μ m.)

a postmortem brain from a patient with double cortex syndrome (*DCX*^{+/-}). The subcortical band in these cases is believed to be comprised of neurons that have arrested prior to reaching the cortical plate due to X chromosome inactivation resulting in a population of neurons without functional DCX. We examined axons in the white matter adjacent to the normal cortex and within the subcortical band with the myelin stain, Luxol fast blue, on paraffin sections (Figures 6D and 6E). Although axons adjacent to the normal white matter appeared fasciculated, the axons in the subcortical band appeared to be disorganized, traveling as single fibers, in random orientations, without evidence of bundling. To label and view axons directly, we placed Dil crystals in the white matter directly adjacent to the abnormal subcortical band as shown in Figure 6F. As a control, axons adjacent to normal cortex (with presumably normal DCX expression) were also labeled with Dil. Axons labeled adjacent to the subcortical band showed striking similarities to mouse *Dcx*^{-/-}; *Dclk*^{-/-}. Unlike the normal axons in the white matter, those within the abnormal subcortical band, arising from *Dcx* negative neurons, traveled as single fibers in random orientations without evidence of bundling. Therefore, in addition to defective migration, human neurons lacking DCX activity appeared to have abnormal axons bearing a striking resemblance to those in the *Dcx*^{-/-}; *Dclk*^{-/-} mouse.

Abnormal Dendritic Morphology and Axon Elongation in *Dcx/Dclk*-Deficient Neurons

We examined cellular morphology of *Dcx*^{-/-}; *Dclk*^{-/-} mutant neurons in dissociated hippocampal cultures at P0. However, because of the limited fertility of compound heterozygote females and the perinatal lethality of *Dcx*^{-/-}; *Dclk*^{-/-} mutants, sufficient samples were difficult to obtain. To further characterize the interaction of *Dcx* and *Dclk* in process formation, we used a *Dcx* RNAi construct (Bai et al., 2003) in *Dclk*^{-/-} embryos co-transfected with a GFP-expressing plasmid as a marker (Matsuda and Cepko, 2004; Takahashi et al., 2002). *Dclk*^{-/-} or wt embryos were transfected by in vivo electroporation at E15 with a *Dcx* RNAi construct, and cortices were dissected out and dissociated the next day. In contrast to the neurons transfected with control RNAi constructs, *Dcx* RNAi treated neurons demonstrated little *Dcx* immunoreactivity (Figure 7A), demonstrating effective knock down of *Dcx* expression.

Neurons from *Dclk*^{-/-} embryos transfected with *Dcx* RNAi showed strikingly aberrant processes in contrast to wt neurons transfected with the *Dcx* RNAi (not shown) and *Dclk*^{-/-} neurons transfected with a control construct (Figure 7B). *Dcx* RNAi-transfected *Dclk*^{-/-} neurons do appear to have a primary axon; however, dendritic processes appear to be shorter and more numerous than in control RNAi-transfected *Dclk*^{-/-}

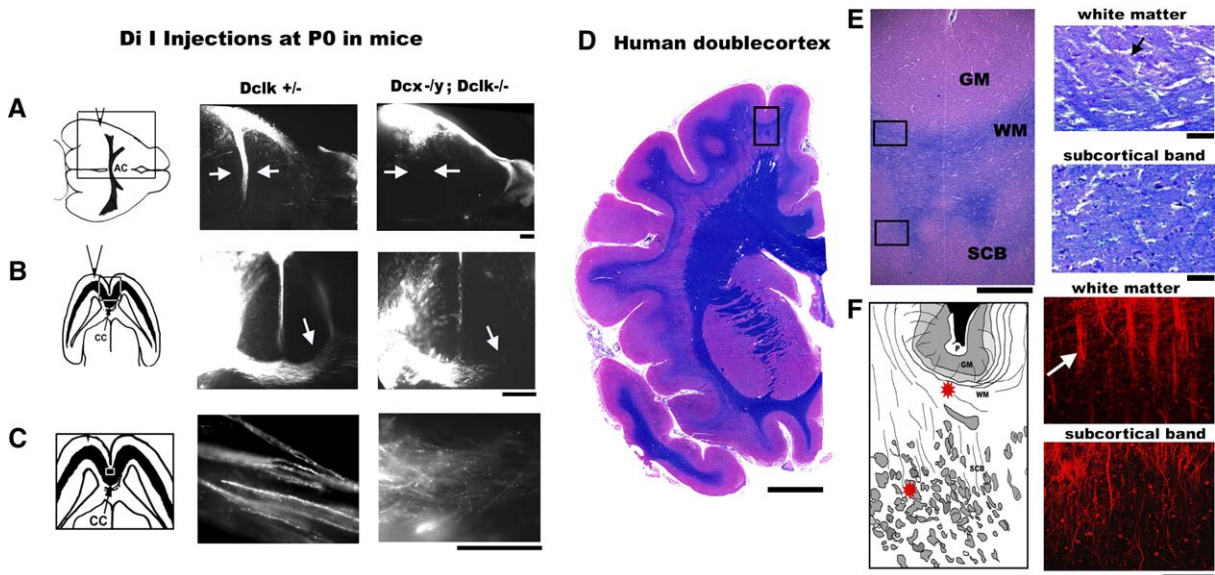


Figure 6. Axonal Defects in *Dcx^{-ly};Dclk^{-/-}* Mice at P0 and in the Human Subcortical Band Heterotopia by Dil Tracing
 (A) Membrane diffusion of Dil after an injection in the entorhinal cortex (diagrammed left) labels axons in the posterior limb of the anterior commissure in control animals (middle). In the mutant mouse, no Dil labeling of axons crossing the midline is seen (right).
 (B) A Dil injection was placed in the left anterior cortex to label the corpus callosum (left). In contrast to the Dil labeled corpus callosum of control animal shown (middle), the axons of the *Dcx^{-ly};Dclk^{-/-}* double knockout mouse cross the midline only sparsely (right).
 (C) A high-power view is taken of the axons in the corpus callosum as shown in the diagram (left). Axons from the control mouse travel in bundles of 5–10 individual fibers (middle). In contrast, the axons from the same site in the *Dcx^{-ly};Dclk^{-/-}* double mutant appear poorly organized, without evidence of fasciculation (left).
 (D) A coronal section of a human brain with subcortical band heterotopia is stained with H&E and luxol fast blue (LFB) for myelin. A rectangle in the frontal cortex marks the region shown in (E) (left).
 (E) The left panel shows a low power view of the normal-appearing cortex (GM) and white matter (WM) and the underlying subcortical band (SCB). Rectangles mark the regions from which high-power views are taken in the white matter and subcortical band. The high-power view of the white matter (top right) shows myelinated axons that travel in fascicles (arrow). In contrast, the high-power view of the subcortical band (bottom right) shows single myelinated axons in many different orientations that are not organized in fascicles.
 (F) Because LFB stains myelin rather than axons directly, we also used Dil to examine axons in both the normal white matter and the subcortical band. The left panel diagrams the location of dil injections (red asterisk). In the white matter, axons are fasciculated (top right), whereas in the subcortical band (bottom right) the axons appear disorganized and look similar to the axons from the mouse in (C). (Scale bars are 400 μ m in [A] and [B], 100 μ m in [C], right panel of [E], and [F]. The scale bar in [D] is 1 cm, and that in the left panel of [E] is 1 mm.)

neurons. Also, in many of these cells a primary dendrite appears to be absent or hypoplastic (yellow arrow) compared to *Dclk^{-/-}* neurons transfected with the control RNAi construct (Figure 7C). We used antisera to MAP2 to examine dendritic structure in a *Dcx^{-ly};Dclk^{-/-}* dissociated hippocampal culture. In this dissociated preparation of double mutant neurons, MAP2 staining revealed cells with aberrantly short dendrites compared to *Dclk^{+/-}* neurons (Figure 7D). The abnormal dendritic structure of *Dcx^{-ly};Dclk^{-/-}* neurons suggests that defects in *Dcx* RNAi-transfected neurons are direct results of *Dcx* inactivation rather than off-target effects of the *Dcx* RNAi construct.

Because the *Dcx^{-ly};Dclk^{-/-}* mutant has widespread defects in white matter tracts, we measured axon length in dissociated cultures to determine whether the RNAi suppression of *Dcx* in *Dclk^{-/-}* embryos resulted in shorter axons as well as dendrites (Figure 7E). In wt neurons, electroporation with the *Dcx* RNAi construct resulted in significantly shorter axons than the control RNAi construct (Figure 7E) ($p \leq 0.003$). However, *Dclk^{-/-}* neurons transfected with the *Dcx* RNAi construct resulted in even further and more significant shortening of axons with a mean length of only 230 μ m compared to a mean of 702 μ m in *Dcx* RNAi-transfected

wild-type neurons (Figure 7E). These data suggest that both *Dcx* and *Dclk* individually have roles in axon elongation but that they complement one another, with simultaneous removal of both causing profound axon defects. These in vitro results also show that *Dcx/Dclk*'s roles in axon outgrowth are largely cell autonomous.

Defective Axonal Expression of Synaptic Vesicle Proteins in *Dcx^{-ly};Dclk^{-/-}* Mutants

Because *Dcx* interacts with vesicle associated proteins, and the link between vesicle trafficking and axon outgrowth (Kimura et al., 2003; Murthy et al., 2003), we examined *Dcx^{-ly};Dclk^{-/-}* tissue for expression of VAMP2 (vesicle-associated membrane protein 2, also known as synaptobrevin) and synaptophysin (syp). VAMP2 is a SNARE (soluble NSF [N-ethylmaleimide-sensitive factor] attachment protein receptor), which is expressed on synaptic vesicles and is critical for vesicle fusion to the presynaptic membrane (Hong, 2005; Kweon et al., 2002; Schoch et al., 2001). Syp, another synaptic vesicle protein, interacts with VAMP2 and is involved in multiple aspects of synaptic vesicle biogenesis, transport, as well as endo- and exocytosis (reviewed in Valtorta et al. [2004]). In contrast to littermate controls and *Dcx^{-ly};Dclk^{+/-}* mice, which showed abundant VAMP2 and syp

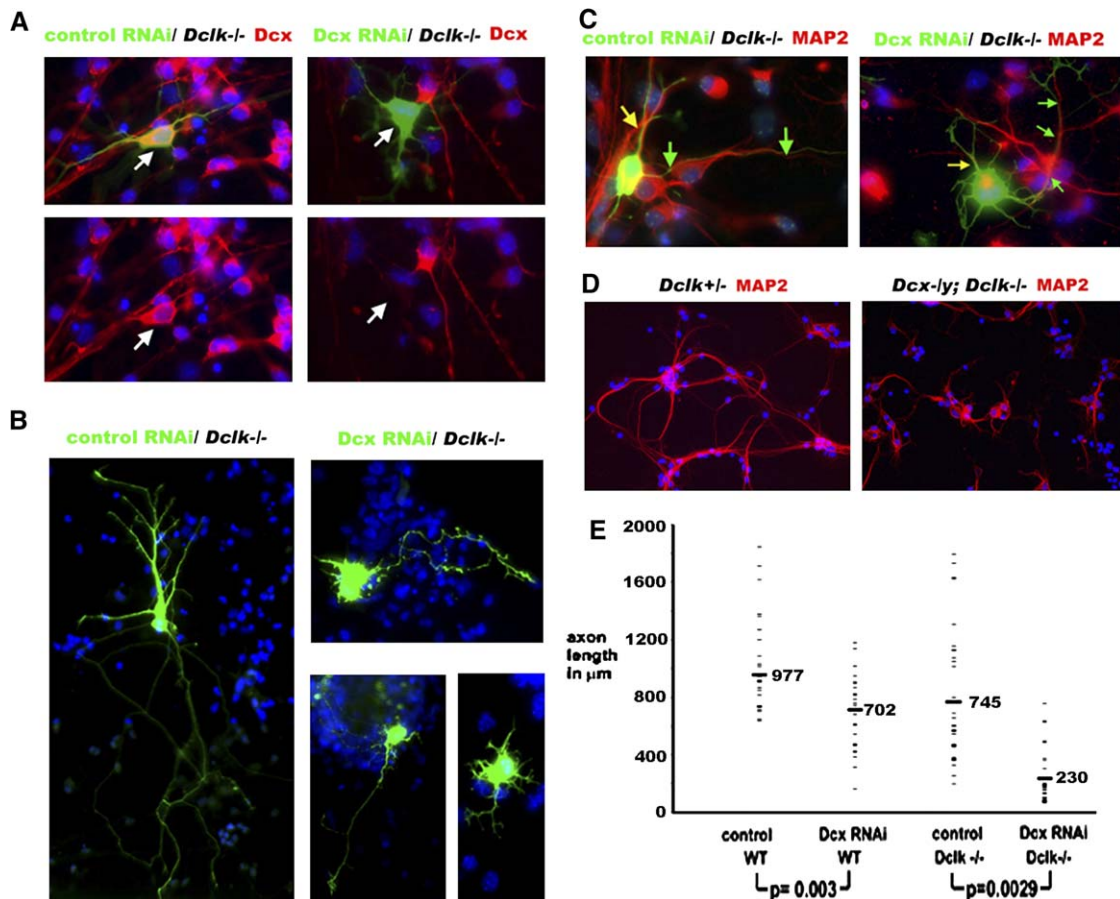


Figure 7. Axonal and Dendritic Abnormalities in *Dcx* RNAi-Transfected *Dclk*^{-/-} Neurons

(A) E15 *Dclk*^{-/-} embryos were transfected with *Dcx* RNAi or a control RNAi along with a marker for transfection, pCAG-GFP, which fills the cell bodies and processes of transfected neurons with GFP. Cortices were dissociated the next day. In control RNAi-transfected neurons (left), GFP-expressing neurons (arrow), *Dcx* expression (red) was unaffected. In contrast, in *Dcx* RNAi-transfected neurons (right), GFP-expressing neurons (arrow) were found to be deficient in *Dcx* expression (red). The top panels show merged images, whereas the bottom panels show only the *Dcx* immunostaining.

(B) In control RNAi-transfected neurons (left), the morphology of pyramidal neurons appears well preserved with a normally appearing dendritic tree and a single long axon. In contrast, *Dclk*^{-/-} neurons transfected with *Dcx* RNAi (right) have abnormally short axons and dendrites. In addition, these neurons appear to have a greater number of processes with more branches than neurons electroporated with the control RNAi construct. (C) MAP-2 staining for dendrites in *Dcx* RNAi-treated *Dclk*^{-/-} neurons (right) demonstrates a paucity of MAP-2-positive structures (yellow arrow) in contrast to the long primary dendrite shown in the control RNAi panel (left). The green arrows indicate the axon, which is MAP-2 negative.

(D) Dissociated neuronal cultures from a *Dcx*^{-/-};*Dclk*^{-/-} mutant (right) and a littermate control (left) shows shorter and fewer MAP-2 positive processes in the *Dcx*^{-/-};*Dclk*^{-/-} mutant.

(E) We quantitated the differences in axonal length in control and *Dcx* RNAi-transfected wild-type and *Dclk*^{-/-} neurons. Axons were measured from the neuronal cell body to the end of the longest branch. Forty randomly chosen axons were measured in each condition and each measurement is graphed with a fine dash. The mean length in μm (thick dash) of the axons in each experimental condition is shown. Axons of *Dcx* RNAi-electroporated neurons in *Dclk*^{-/-} mice (mean, 230 μm) are shorter than that of control RNAi neurons in *Dclk*^{-/-} mice (mean, 745 μm) with most of the *Dcx* RNAi axonal measurements clustered under 200 μm ($p = 0.0029$ by Student's *t* test). *Dcx* RNAi transfection of wild-type neurons results in shorter axons than control RNAi (mean 977 versus 702 μm , $p = 0.003$); however, *Dcx* RNAi in wild-type neurons does not have as much of an effect on axon length as *Dcx* RNAi in *Dclk*^{-/-} neurons.

immunoreactivity in both the marginal zone and subplate, *Dcx*^{-/-};*Dclk*^{-/-} mutants had consistent, dramatically decreased VAMP2 staining throughout the cortex at P0 in three separate animals tested (Figures 8A and 8B). Because of the known defect in axon elongation, the lack of VAMP2 and syp might be due to a paucity of axons growing into the subplate, so we costained with tau-1 to label axons in the same sections. In contrast to VAMP2, tau-1 staining in the cortex in *Dcx*^{-/-};*Dclk*^{-/-} mice did not differ appreciably from controls, suggesting that tau-positive axons in the mutant cortex were deficient in VAMP2 and syp.

In dissociated cultures of *Dcx*/*Dclk*-deficient neurons the subcellular localization of both VAMP2 and syp was also strikingly different from control neurons (Figures 8C and 8D). *Dclk*^{-/-} neurons were transfected with either *Dcx* RNAi or control RNAi as described above and then immunostained with antisera for VAMP2, syp, or syntaxin 3, another SNARE which is expressed in the target membrane (Hong, 2005). In *Dclk*^{-/-} neurons transfected with control RNAi, both VAMP2 and syp expression localized to the axons, as well as neuronal cell bodies (Figure 8C). In contrast, although high levels of both proteins were detected in cell bodies by immunocytochemistry,

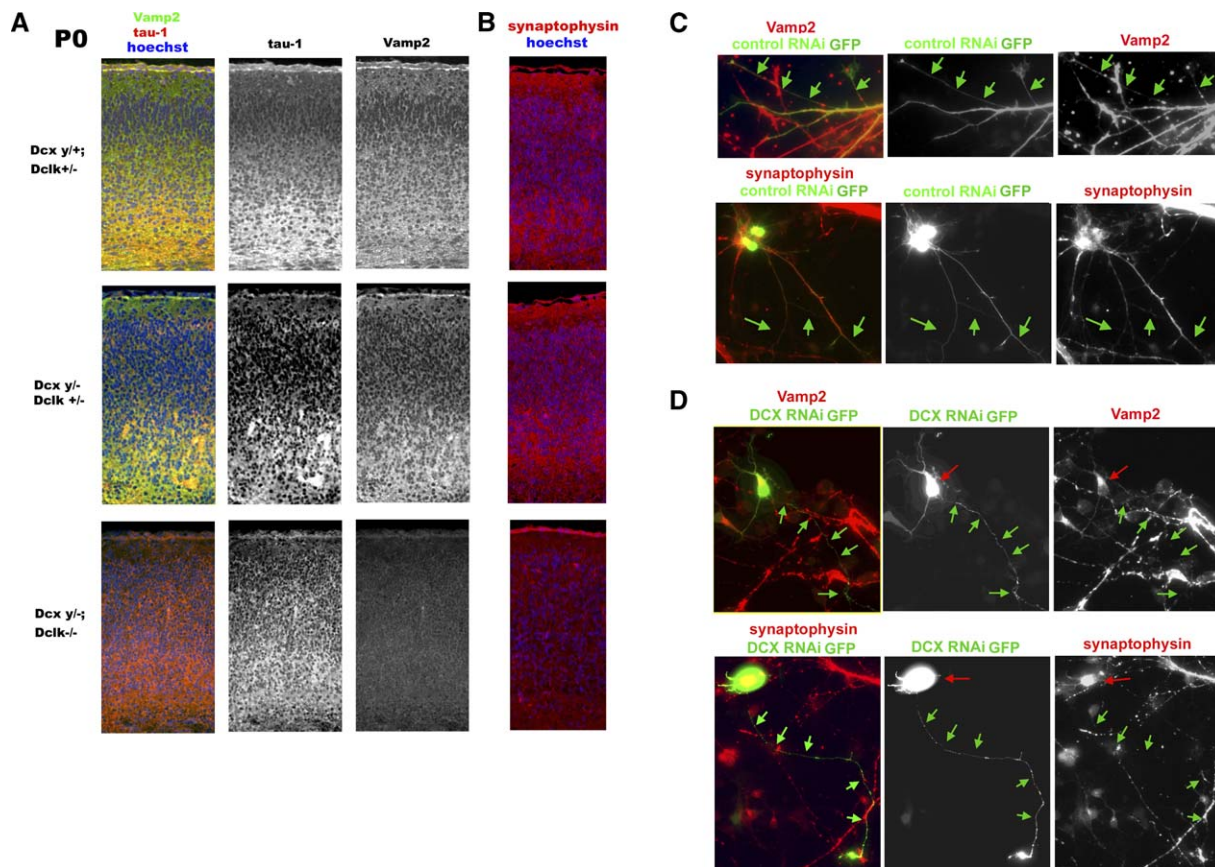


Figure 8. Decreased VAMP2 and Syp Immunoreactivity in *Dcx^{-ly};Dclk^{-/-}* Mice

(A) Sections through the cerebral cortex of *Dclk^{+/-}*, *Dcx^{-ly};Dclk^{+/-}*, and *Dcx^{-ly};Dclk^{-/-}* mice at P0 are immunostained for tau and the synaptic vesicle protein, VAMP2. Although tau staining for axons in the cortex demonstrates little difference between *Dclk^{+/-}*, *Dcx^{-ly};Dclk^{+/-}*, and *Dcx^{-ly};Dclk^{-/-}* mice, VAMP staining is almost entirely absent in the *Dcx^{-ly};Dclk^{-/-}* mutant in contrast to *Dclk^{+/-}* and *Dcx^{-ly};Dclk^{+/-}* littermates.

(B) Immunoreactivity to syp, another synaptic vesicle protein, appears to be greatly reduced in *Dcx^{-ly};Dclk^{-/-}* animals as compared to *Dclk^{+/-}* and *Dcx^{-ly};Dclk^{+/-}* mice (middle).

(C) Immunoreactivity for synaptic vesicle proteins, VAMP2 (top row) and syp (bottom row) in dissociated cultures of *Dclk^{-/-}* neurons transfected with control RNAi and CAG-GFP (as described in Figure 7) shows that in control transfected cells, both VAMP2 and syp immunostaining colocalize in axons (green arrows), as well as cell bodies (not shown for VAMP2).

(D) In *Dcx* RNAi-transfected *Dclk^{-/-}* neurons, however, both VAMP2 (top) and syp (bottom) show high levels of both in cell bodies (red arrows). However, levels in axons (green arrows) of *Dcx* RNAi-transfected neurons are not detectable.

VAMP2 and syp were almost entirely absent from axons in *Dcx* RNAi-transfected neurons (Figure 8D). In contrast, syntaxin 3, a SNARE protein not expressed on vesicles, but rather on the presynaptic target membrane, appears to localize normally to both axons and cell bodies (Supplemental Data). These data again suggest that *Dcx* and *Dclk* have essential roles in the transport of VAMP2- and syp-positive vesicles from the cell body to the axon.

Discussion

Here, we created mutant mice in both *Dcx* and *Dclk* and showed that these *Dcx^{-ly};Dclk^{-/-}* double mutant mice have more severe defects in neuronal migration than in either mutant alone. Whereas the *Dclk* mutant shows grossly normal cortical layering and the *Dcx* mutant shows mild disruption of layering in the hippocampus, the *Dcx^{-ly};Dclk^{-/-}* double mutant demonstrates profound disruption of the hippocampus, defective neuronal migration in the cingulate gyrus, and defects in migration of later-born layers throughout the neocortex. In

addition, the double mutant has widespread disruption of white-matter tracts, including partial agenesis of the corpus callosum, absence of the anterior commissure, and abnormalities in the internal capsule. Studies in dissociated cultures showed surprising defects in both axon elongation as well as dendritic morphology. Examination of synaptic vesicle proteins revealed defects in vesicular trafficking in axons, which may explain both the defects in neuronal migration and axon outgrowth.

Comparison of the *Dcx*/*Dclk* Mutant Mice to Human XLIS

The *Dcx^{-ly};Dclk^{-/-}* double mutant has features similar to human XLIS, including a lamination defect in the neocortex. Although cortical lamination in XLIS was originally described as a simplified, thickened four-layered cortex (Berg et al., 1998; Ross et al., 1997), a more recent case describes a six-layered cortex (Viot et al., 2004). The *Dcx^{-ly};Dclk^{-/-}* mutant demonstrates a neuronal migration defect without a clear inversion of cortical lamination. The mouse double mutant also demonstrates some variability in lamination—most notably in the

appearance of the marginal zone. Women who are heterozygous for *DCX* have a subcortical band heterotopia beneath a relatively normal appearing cortex and normal ventricular size and conformation. Unlike *DCX*^{+/-} women, the *Dcx*^{+/-};*Dclk*^{-/-} female mouse does not resemble “double cortex” syndrome, nor have we seen axonal outgrowth defects. These species differences are not unique to mice versus humans because mice and rats show some difference in the effect of *Dcx* inactivation as well (Bai et al., 2003), though the reasons for these species differences are not known.

In addition to the neuronal migration phenotype, the *Dcx*^{-/y};*Dclk*^{-/-} mouse has a profound disruption of white-matter tract formation. In humans, a reduced volume in white matter has been documented by both MRI and in pathological cases of XLIS (Berg et al., 1998; Ross et al., 1997; Viot et al., 2004); however, the axonal phenotypes have been more difficult to study. Our analysis of axons from a human specimen with subcortical band heterotopia has shown some remarkable similarities between axons in the subcortical band and those in the *Dcx*^{-/y};*Dclk*^{-/-} mutants. In both the human and the mouse, axons form few or abnormal fascicles. Thus, it appears in both the human syndrome and the animal model, *Dcx* and *Dclk* have a role in axon outgrowth as well as neuronal migration.

Dcx and Cytoskeletal Regulation in Migration and Neural Process Formation

Although *Dcx* binding is known to stabilize microtubules (Gleeson et al., 1999), the exact function of doublecortin domains in mediating either neuronal migration or axonal outgrowth is unknown and much of the recent work focuses on *Dcx* regulation of the cytoskeleton. A recent report demonstrates *Dcx* binding to filamentous actin in addition to microtubules (Tsukada et al., 2005). *Dcx* has been shown to interact with neurabin II, a protein phosphatase known to regulate dendritic morphology (Feng et al., 2000b). The binding of *Dcx* to filamentous actin is enhanced through this interaction with neurabin II (Tsukada et al., 2005). These data suggest that *Dcx* may function in migration and axon outgrowth by facilitating the cross talk between the actin and tubulin cytoskeleton during these processes.

Dcx/*Dclk*-deficient axons and growth cones may be unable to coordinate actin/microtubule dynamics resulting in the inability to respond to guidance cues. These mutant growth cones may demonstrate defects in reaching targets such as the midline or even in fascicle formation as observed in *Dcx*^{-/y};*Dclk*^{-/-} mice. *Dcx* may be involved in the steps of neuronal migration in which neurons transform from a multipolar shape to a bipolar shape (Noctor et al., 2004) essential for it to traverse the cortical plate (LoTurco, 2004). In rat cortical neurons in which *Dcx* has been inhibited by RNAi, migrating cells arrested beneath the cortex show a persistently multipolar morphology (Bai et al., 2003). Transformation of this multipolar cell into a bipolar shape may be through *Dcx*-mediated regulation of actin and tubulin.

Dcx Family Proteins in Vesicle Transport

Our studies demonstrate a paucity of two vesicle proteins, *syp* and *VAMP2*, in the axons of *Dcx* RNAi-treated *Dclk*^{-/-} neurons. This defect in vesicle protein localiza-

tion may reflect the destabilization or dysregulation of microtubules caused by *Dcx*/*Dclk* deficiency because vesicle sorting and transport are microtubule-dependent processes. The destabilization of microtubules alone caused by mutations in other MAP's cause dramatic effects on axon elongation. Thus, the aberrant sorting/transport of vesicles in *Dcx*/*Dclk*-deficient neurons may be merely an indirect effect of the disrupted microtubule cytoskeleton, and the vesicle transport defect need not be the primary cause of impaired axon outgrowth in these neurons.

Alternatively, *Dcx*/*Dclk* may have a direct role in vesicle sorting or transport through specific interactions with other proteins in these pathways. *Dcx* and *Dclk* interact with μ subunits of clathrin adaptor complexes, and these complexes colocalize with *Dcx* proteins along neurites and within growth cones (Friocourt et al., 2001). *Dcx* proteins may link vesicles to microtubules by binding tubulin at the N terminus and vesicle-associated proteins such as the clathrin adaptor complexes through its C terminus (Friocourt et al., 2001). Interestingly, *Cdk5*, a kinase essential in neuronal migration (Gilmore et al., 1998; Ohshima et al., 1996), regulates *Dcx* affinity for microtubules (Tanaka et al., 2004) and has also been implicated in the regulation of vesicular trafficking. RNAi for *Cdk5* or *p35* blocks vesicle formation in the Golgi apparatus (Paglini et al., 2001), regulates synaptic vesicle endocytosis (reviewed in Nguyen and Bibb [2003]), and regulates synaptic vesicle fusion (Barclay et al., 2004).

Defective vesicle transport during development may result in impaired membrane expansion at the growth cone of the axon or the leading edge of a migrating neuron (Kimura et al., 2003; Shirasu et al., 2000). SNARES such as *VAMP2* have been implicated in neurite outgrowth in PC-12 cells (Kimura et al., 2003; Shirasu et al., 2000) so that the paucity of vesicles in the *Dcx*/*Dclk* double mutant axons may produce the abnormal axons observed. The role of *Dcx* in membrane extension via vesicle trafficking may explain the neuronal migration defect, as well, because migrating neurons undergo a change in shape, requiring membrane biogenesis and redistribution, in order to elaborate the leading process that guides migration into the cortical plate.

Experimental Procedures

In Situ Hybridization and Immunohistochemistry

E12.5, E14.5, E16.5, E17.5, P0.5, and adult Swiss Webster mice (Taconic, Germantown, NY) were sacrificed. Animal-use procedures were reviewed and approved by the Harvard Medical School Standing Committee on Animals and were in accordance with the National Institutes of Health Guide for the Care and Use of Laboratory Animals. Nonradioactive ISH was performed as described (Berger and Hediger, 2001) with digoxigenin (DIG)-labeled cRNA probes. *Dclk* probe was designed to recognize all transcripts except *CARP* and transcribed from a PCR-amplified fragment of 3'UTR of *Dclk* genomic DNA with the primers: 5'-AATTAACCCTCACTAAAGGGCCGA TTCCATGGTAACTCTAGG-3' *DCLK*. T7: 5'-GTAATACACTACTATA GGGCCAGCAGCTGCAGATCAGTGT-3'. Sections were hybridized at 68°C for 72 hr (probe concentration 100 ng/ml). Sense probe transcript was used as a control.

Gene Targeting and Generation of *Dclk* Mutant Mice

The starting vector was pSAGalpgkneo2PGKDTA (gift from Sheila Thomas, Beth Israel Deaconess Medical Center, Boston, MA), which contains a splice acceptor *lacZ*, a phosphoglycerate kinase (PGK)-neo cassette flanked by short polylinker sites, and a PGK-diphtheria

toxin cassette. A 2.9 kb EcoRV fragment from the genomic region 5' of exon 9 of *Dclk* was subcloned into the SmaI site to form the 5' arm of the targeting construct, and a 4.5 kb XbaI fragment 3' of exon 11 was subcloned into the NheI site of the resultant plasmid to form the 3' arm of the targeting construct. This vector was linearized with NotI and transfected into TC1 embryonic stem (ES) cells as described (Deng et al., 1994). Correct targeting of *Dclk* was identified by Southern blotting of NheI-digested genomic DNA with a 400bp NotI/EcoRV probe derived from a subcloned genomic fragment upstream of the 5' arm of the targeting construct. Positive ES cell clones were injected into 129/SvJ blastocysts, and germline transmission was obtained. We established the *Dclk* mutant allele in a mixed (129/SvJ/C57BL/6J) background. Genotyping was subsequently performed by PCR with pairs of primers specific for exon 9 of *Dclk* (DCLK.WT1: ATGGGGGTGATTTGATTTGA; DCLK.WT2: GACAACCTGAAGACAGGGGA) and for a region spanning from 5' of exon 9 to the Neo cassette of the targeting construct (DCLK.5'one: GCTCTGACACTGAACGGACA; PGK.Neo.5': CAGAAAGCGAAGGAGCAAAG).

Western Blot Analysis

Total brain protein extracts from adult littermate animals were extracted, and Western analysis performed with anti-Dclk N-terminal (Lin et al., 2000) rabbit antiserum, 1:500; (Mizuguchi et al., 1999) rabbit antiserum, 1:500 (gift of M. Mizuguchi and S. Takashima); or C-terminal (Burgess et al., 1999) c16-3998 affinity-purified rabbit IgG antibody (gift of O. Reiner). Rabbit anti-tubulin antibody (1:5000; Chemicon, Temecula, CA) was used as a loading control.

Histologic and Immunohistochemical Analysis

Sections were stained with hematoxylin and eosin (H&E). For immunohistochemistry, we used the following primary antibodies: anti-Cux-1, rabbit IgG, 1:500; G10 antibody, 1:500, mouse IgG (gift of A.M. Goffinet); anti-Foxp1, rabbit IgG, 1:200; anti-Foxp2, rabbit IgG, 1:200; anti-tau-1, mouse IgG, 1:200 (Chemicon); anti-MAP2, mouse IgG 2a, 1:200 (Sigma); anti-VAMP2, mouse IgG 1:200 (Sy sy); anti-Syntaxin3, rabbit IgG, 1:100 (Sy sy).

Fluorescent Layer-Specific Marker Strain

Dclk mutants were mated to male mice carrying a Thy1-yellow fluorescent protein (YFP) transgene (The Jackson Laboratory, Bar Harbor, ME) (strain name: B6.Cg-TgN[Thy1-YFP-H]2Jrs) that produces YFP expression predominantly in a subset of cerebral cortical layer 5 pyramidal cells (YFP-G in Feng et al. [2000a]). Typing was performed by PCR as described (Feng et al., 2000a).

Dye Tracing

Brains from (P0) animals fixed in 4% PFA were dye labeled with a single crystal Fast Dil (1,1'-dilinoleyl-3,3',3'-tetramethyl-indocarbocyanine 4-chlorobenzenesulfonate) (Molecular Probes, Eugene, OR) implanted into the cortical layer of frontal cortex, olfactory bulb, or entorhinal cortex, respectively. Labeled brains were incubated at 37°C for 14 days, and 100 μ m axial vibratome sections were taken.

Dcx RNA Interference Constructs and In Utero Electroporation

Both the Dcx RNAi (hp) and the control RNAi (m3) constructs are based on the mU6pro vector (Bai et al., 2003). To fluorescently label transfected cells, pCAG-GFP (Matsuda and Cepko, 2004) was co-transfected with the RNAi constructs at 0.5 mg/ml. Plasmids were transfected by in utero electroporation. Briefly, pregnant Swiss Webster or *Dclk*^{-/-} mice were euthanized at E15, and embryos removed. Lateral ventricles were injected with pulled glass microcapillary needles with plasmids in a 0.01% fast green solution (Sigma). Electrodes were placed on either side of the embryo's head, and 5 \times 100 ms square pulses at 40 v were administered at 950 ms intervals with a BTX830 square-wave pulse generator (Genetronics, Harvard Apparatus). Cortices were dissected and maintained on organotypic culture membranes for 24 hr, and GFP expression was visualized, and tissue was dissociated with papain digestion and trituration. Neurons were plated on 12 mm cover slips at high density and examined after 5–6 days.

Supplemental Data

The Supplemental Data for this article can be found online at <http://www.neuron.org/cgi/content/full/49/1/41/DC1/>.

Acknowledgments

We would like to thank members of the Walsh Lab for their help and Seonhee Kim for advice during all stages of this work. The pCAG-GFP vector was provided by T. Matsuda and C. Cepko (Harvard Medical School). The C-terminal antibody for Dclk was provided by O. Reiner (Weizman Institute, Israel), and the N-terminal antibody was provided by M. Mizuguchi and S. Takashima (Jichi Medical School, Japan). *Dcx* RNAi and control RNAi constructs were provided by J. LoTurco (University of Connecticut). G10 antibody was provided by A. Goffinet (University of Louvain Medical School, Belgium). T.A.S.D. was supported by the Adams Quan fellowship and by the Harvard Center for Neurodegeneration and Repair. J.S.L. was supported by the Clinical Investigator Training Program: Beth Israel Deaconess Medical Center—Harvard/MIT Health Sciences and Technology, in collaboration with Pfizer Inc. and Merck & Co. S.-Y.Y. is a postdoctoral research associate, and C.A.W. is an Investigator of the Howard Hughes Institute of Medicine. C.A.W. was supported by National Institute of Neurological Disorders and Stroke (P01 NS40043).

Received: April 21, 2005

Revised: September 22, 2005

Accepted: October 26, 2005

Published: January 4, 2006

References

- Bai, J., Ramos, R.L., Ackman, J.B., Thomas, A.M., Lee, R.V., and LoTurco, J.J. (2003). RNAi reveals doublecortin is required for radial migration in rat neocortex. *Nat. Neurosci.* 6, 1277–1283.
- Barclay, J.W., Aldea, M., Craig, T.J., Morgan, A., and Burgoyne, R.D. (2004). Regulation of the fusion pore conductance during exocytosis by cyclin-dependent kinase 5. *J. Biol. Chem.* 279, 41495–41503.
- Berg, M.J., Schifitto, G., Powers, J.M., Martinez-Capolino, C., Fong, C.T., Myers, G.J., Epstein, L.G., and Walsh, C.A. (1998). X-linked female band heterotopia-male lissencephaly syndrome. *Neurology* 50, 1143–1146.
- Berger, U.V., and Hediger, M.A. (2001). Differential distribution of the glutamate transporters GLT-1 and GLAST in tanycytes of the third ventricle. *J. Comp. Neurol.* 433, 101–114.
- Burgess, H.A., and Reiner, O. (2000). Doublecortin-like kinase is associated with microtubules in neuronal growth cones. *Mol. Cell. Neurosci.* 16, 529–541.
- Burgess, H.A., and Reiner, O. (2001). Cleavage of doublecortin-like kinase by calpain releases an active kinase fragment from a microtubule anchorage domain. *J. Biol. Chem.* 276, 36397–36403.
- Burgess, H.A., and Reiner, O. (2002). Alternative splice variants of doublecortin-like kinase are differentially expressed and have different kinase activities. *J. Biol. Chem.* 277, 17696–17705.
- Burgess, H.A., Martinez, S., and Reiner, O. (1999). KIAA0369, doublecortin-like kinase, is expressed during brain development. *J. Neurosci. Res.* 58, 567–575.
- Caviness, V.S., Jr. (1982). Neocortical histogenesis in normal and reeler mice: a developmental study based upon [3H]thymidine autoradiography. *Brain Res.* 256, 293–302.
- Corbo, J.C., Deuel, T.A., Long, J.M., LaPorte, P., Tsai, E., Wynshaw-Boris, A., and Walsh, C.A. (2002). Doublecortin is required in mice for lamination of the hippocampus but not the neocortex. *J. Neurosci.* 22, 7548–7557.
- de Bergueyck, V., Naerhuyzen, B., Goffinet, A.M., and Lambert de Rouvroit, C. (1998). A panel of monoclonal antibodies against reelin, the extracellular matrix protein defective in reeler mutant mice. *J. Neurosci. Methods* 82, 17–24.
- Deng, C.X., Wynshaw-Boris, A., Shen, M.M., Daugherty, C., Ornitz, D.M., and Leder, P. (1994). Murine FGFR-1 is required for early post-implantation growth and axial organization. *Genes Dev.* 8, 3045–3057.
- des Portes, V., Pinard, J.M., Billuart, P., Vinet, M.C., Koulakoff, A., Carrie, A., Gelot, A., Dupuis, E., Motte, J., Berwald-Netter, Y., et al. (1998). A novel CNS gene required for neuronal migration and

- involved in X-linked subcortical laminar heterotopia and lissencephaly syndrome. *Cell* 92, 51–61.
- Dobyns, W.B., Andermann, E., Andermann, F., Czapanzky-Beilman, D., Dubeau, F., Dulac, O., Guerrini, R., Hirsch, B., Ledbetter, D.H., Lee, N.S., et al. (1996). X-linked malformations of neuronal migration. *Neurology* 47, 331–339.
- Feng, G., Mellor, R.H., Bernstein, M., Keller-Peck, C., Nguyen, Q.T., Wallace, M., Nerbonne, J.M., Lichtman, J.W., and Sanes, J.R. (2000a). Imaging Neuronal Subsets in Transgenic Mice Expressing Various Spectral Variants of GFP. *Neuron* 28, 41–51.
- Feng, J., Yan, Z., Ferreira, A., Tomizawa, K., Liauw, J.A., Zhuo, M., Allen, P.B., Ouimet, C.C., and Greengard, P. (2000b). Spinophilin regulates the formation and function of dendritic spines. *Proc. Natl. Acad. Sci. USA* 97, 9287–9292.
- Ferland, R.J., Cherry, T.J., Preware, P.O., Morrissey, E.E., and Walsh, C.A. (2003). Characterization of *Foxp2* and *Foxp1* mRNA and protein in the developing and mature brain. *J. Comp. Neurol.* 460, 266–279.
- Francis, F., Koulakoff, A., Boucher, D., Chafey, P., Schaar, B., Vinet, M.C., Friocourt, G., McDonnell, N., Reiner, O., Kahn, A., et al. (1999). Doublecortin is a developmentally regulated, microtubule-associated protein expressed in migrating and differentiating neurons. *Neuron* 23, 247–256.
- Friocourt, G., Chafey, P., Billuart, P., Koulakoff, A., Vinet, M.C., Schaar, B.T., McConnell, S.K., Francis, F., and Chelly, J. (2001). Doublecortin interacts with mu subunits of clathrin adaptor complexes in the developing nervous system. *Mol. Cell. Neurosci.* 18, 307–319.
- Gilmore, E.C., Ohshima, T., Goffinet, A.M., Kulkarni, A.B., and Herup, K. (1998). Cyclin-dependent kinase 5-deficient mice demonstrate novel developmental arrest in cerebral cortex. *J. Neurosci.* 18, 6370–6377.
- Gleeson, J.G., Allen, K.M., Fox, J.W., Lamperti, E.D., Berkovic, S., Scheffer, I., Cooper, E.C., Dobyns, W.B., Minnerath, S.R., Ross, M.E., and Walsh, C.A. (1998). Doublecortin, a brain-specific gene mutated in human X-linked lissencephaly and double cortex syndrome, encodes a putative signaling protein. *Cell* 92, 63–72.
- Gleeson, J.G., Lin, P.T., Flanagan, L.A., and Walsh, C.A. (1999). Doublecortin is a microtubule-associated protein and is expressed widely by migrating neurons. *Neuron* 23, 257–271.
- Havroni, D., Rattner, A., Bundman, M., Lederfein, D., Gabarah, A., Mangelus, M., Silverman, M.A., Kedar, H., Naor, C., Kornuc, M., et al. (1998). Hippocampal plasticity involves extensive gene induction and multiple cellular mechanisms. *J. Mol. Neurosci.* 10, 75–98.
- Hong, W. (2005). SNAREs and traffic. *Biochim. Biophys. Acta* 1744, 493–517.
- Kim, M.H., Cierpicki, T., Derewenda, U., Krowarsch, D., Feng, Y., Devedjiev, Y., Dauter, Z., Walsh, C.A., Otlewski, J., Bushweller, J.H., and Derewenda, Z.S. (2003). The DCX-domain tandems of doublecortin and doublecortin-like kinase. *Nat. Struct. Biol.* 10, 324–333.
- Kimura, K., Mizoguchi, A., and Ide, C. (2003). Regulation of growth cone extension by SNARE proteins. *J. Histochem. Cytochem.* 51, 429–433.
- Kweon, D.H., Kim, C.S., and Shin, Y.K. (2002). The membrane-dipped neuronal SNARE complex: a site-directed spin labeling electron paramagnetic resonance study. *Biochemistry* 41, 9264–9268.
- Lin, P.T., Gleeson, J.G., Corbo, J.C., Flanagan, L., and Walsh, C.A. (2000). DCAMKL1 encodes a protein kinase with homology to doublecortin that regulates microtubule polymerization. *J. Neurosci.* 20, 9152–9161.
- LoTurco, J. (2004). Doublecortin and a tale of two serines. *Neuron* 41, 175–177.
- Matsuda, T., and Cepko, C.L. (2004). Electroporation and RNA interference in the rodent retina in vivo and in vitro. *Proc. Natl. Acad. Sci. USA* 101, 16–22.
- Mizuguchi, M., Qin, J., Yamada, M., Ikeda, K., and Takashima, S. (1999). High expression of doublecortin and KIAA0369 protein in fetal brain suggests their specific role in neuronal migration. *Am. J. Pathol.* 155, 1713–1721.
- Murthy, M., Garza, D., Scheller, R.H., and Schwarz, T.L. (2003). Mutations in the exocyst component Sec5 disrupt neuronal membrane traffic, but neurotransmitter release persists. *Neuron* 37, 433–447.
- Nguyen, C., and Bibb, J.A. (2003). Cdk5 and the mystery of synaptic vesicle endocytosis. *J. Cell Biol.* 163, 697–699.
- Nieto, M., Monuki, E.S., Tang, H., Imitola, J., Haubst, N., Khoury, S.J., Cunningham, J., Gotz, M., and Walsh, C.A. (2004). Expression of *Cux-1* and *Cux-2* in the subventricular zone and upper layers II–IV of the cerebral cortex. *J. Comp. Neurol.* 479, 168–180.
- Noctor, S.C., Martinez-Cerdeno, V., Ivic, L., and Kriegstein, A.R. (2004). Cortical neurons arise in symmetric and asymmetric division zones and migrate through specific phases. *Nat. Neurosci.* 7, 136–144.
- Ohshima, T., Ward, J.M., Huh, C.G., Longenecker, G., Veeranna, Pant H.C., Brady, R.O., Martin, L.J., and Kulkarni, A.B. (1996). Targeted disruption of the cyclin-dependent kinase 5 gene results in abnormal corticogenesis, neuronal pathology and perinatal death. *Proc. Natl. Acad. Sci. USA* 93, 11173–11178.
- Paglini, G., Peris, L., Diez-Guerra, J., Quiroga, S., and Caceres, A. (2001). The Cdk5-p35 kinase associates with the Golgi apparatus and regulates membrane traffic. *EMBO Rep.* 2, 1139–1144.
- Ross, M.E., Allen, K.M., Srivastava, A.K., Featherstone, T., Gleeson, J.G., Hirsch, B., Harding, B.N., Andermann, E., Abdullah, R., Berg, M., et al. (1997). Linkage and physical mapping of X-linked lissencephaly/SBHD (XLIS): a gene causing neuronal migration defects in human brain. *Hum. Mol. Genet.* 6, 555–562.
- Schoch, S., Deak, F., Konigstorfer, A., Mozhayeva, M., Sara, Y., Sudhof, T.C., and Kavalali, E.T. (2001). SNARE function analyzed in synaptobrevin/VAMP knockout mice. *Science* 294, 1117–1122.
- Shirasu, M., Kimura, K., Kataoka, M., Takahashi, M., Okajima, S., Kawaguchi, S., Hirasawa, Y., Ide, C., and Mizoguchi, A. (2000). VAMP-2 promotes neurite elongation and SNAP-25A increases neurite sprouting in PC12 cells. *Neurosci. Res.* 37, 265–275.
- Silverman, M.A., Benard, O., Jaaro, H., Rattner, A., Citri, Y., and Seger, R. (1999). cPG16, a novel protein serine/threonine kinase downstream of cAMP-dependent protein kinase. *J. Biol. Chem.* 274, 2631–2636.
- Sossey-Alaoui, K., and Srivastava, A.K. (1999). DCAMKL1, a brain-specific transmembrane protein on 13q12.3 that is similar to doublecortin (DCX). *Genomics* 56, 121–126.
- Takahashi, M., Sato, K., Nomura, T., and Osumi, N. (2002). Manipulating gene expressions by electroporation in the developing brain of mammalian embryos. *Differentiation* 70, 155–162.
- Tanaka, T., Serneo, F.F., Tseng, H.C., Kulkarni, A.B., Tsai, L.H., and Gleeson, J.G. (2004). Cdk5 phosphorylation of doublecortin ser297 regulates its effect on neuronal migration. *Neuron* 41, 215–227.
- Taylor, K.R., Holzer, A.K., Bazan, J.F., Walsh, C.A., and Gleeson, J.G. (2000). Patient mutations in doublecortin define a repeated tubulin-binding domain. *J. Biol. Chem.* 275, 34442–34450.
- Tsukada, M., Prokscha, A., Ungewickell, E., and Eichele, G. (2005). Doublecortin association with actin filaments is regulated by Neurexin II. *J. Biol. Chem.* 280, 11361–11368.
- Valtorta, F., Pennuto, M., Bonanomi, D., and Benfenati, F. (2004). Synaptophysin: leading actor or walk-on role in synaptic vesicle exocytosis? *Bioessays* 26, 445–453.
- Viot, G., Sonigo, P., Simon, I., Simon-Bouy, B., Chadeyron, F., Beldjord, C., Tantau, J., Martinovic, J., Esculpavit, C., Brunelle, F., et al. (2004). Neocortical neuronal arrangement in LIS1 and DCX lissencephaly may be different. *Am. J. Med. Genet. A* 126, 123–128.
- Vreugdenhil, E., Datson, N., Engels, B., de Jong, J., van Koningsbruggen, S., Schaaf, M., and de Kloet, E.R. (1999). Kainate-elicited seizures induce mRNA encoding a CaMK-related peptide: a putative modulator of kinase activity in rat hippocampus. *J. Neurobiol.* 39, 41–50.